Indirect exciton fine structure in GaP and the effect of uniaxial stress

R. G. Humphreys,* U. Rössler,† and M. Cardona
Max-Planck-Institut für Festkörperforschung, 7 Stuttgart 80, Federal Republic of Germany
(Received 5 June 1978)

The technique of high-resolution wavelength-modulated absorption has been used to study the indirect exciton in GaP, both with and without uniaxial stress. The existence of a camel's back in the exciton dispersion curves is confirmed, and its height at zero stress is found to be 2.4 ± 0.2 meV for the lower (X_7) exciton ground state and slightly larger for the upper (X_6) exciton. The valley-anisotropy splitting between these states at zero stress is found to be 1.9 ± 0.2 meV at the minima of the dispersion curves. The observed changes in exciton binding energy with stress are treated approximately using perturbation theory. The following deformation potentials are found: $b = -1.8 \pm 0.2$ eV, $d = -4.5 \pm 0.5$ eV, $\mathcal{E}_2 = 6.5 \pm 0.5$ eV, $\mathcal{E}_1 - a = 1.6 \pm 0.2$ eV. The exciton parameters obtained rest mainly on the results for [001] stress, as the other stress directions (particularly [111]) give complex line shapes which cannot be understood with a simple model. The observation of an excited state in pure material is found to imply a mean group-state binding energy of 20.5 meV, in good agreement with recent theoretical calculations, but higher than many experimental estimates. The binding energy is confirmed to be of this magnitude from level-crossing effects in the stress measurements.

I. INTRODUCTION

Indirect excitons in tetrahedral semiconductors have been the subjects of considerable recent theoretical[1-4] and experimental[5-8] interest. This has been partly stimulated by the observation of electron-hole drop formation phenomena[9,10] and partly by improvements in theory and in experiment (particularly sample quality), which have permitted a better understanding of these fundamental electronic excitations. So far, theoretical results and experimental data agree in great detail for Ge,[4,5] and to some extent for Si.[6-8]

The problem in GaP is more complicated. More than ten years ago careful absorption measurements showed the presence of unassigned fine structure at the absorption edge.[11] The suggestion was made that this might be due to anomalous structure in the exciton dispersion curve. No further experimental evidence on this point was obtained until the observation of phonon sidebands in bound exciton luninescence was recently attributed to intervalley g-type scattering[12] indicating that the conduction-band minima are close to, but not at, the zone boundary. This gives rise to a "camel's back" structure in the conduction band, as had been suggested by Lawaetz.[13] Kopylov and Pikhtin[14] have shown that it is necessary to include a camel's back, in order to explain the experimentally observed energies of donor excited states.

Calculations of the exciton binding energy and valley-anisotropy splitting in GaP neglecting the camel's back have been published.[1,2] Very recently a calculation has been performed which includes the camel's back structure.[3]

The lowest band gap in GaP is between the zone-center degenerate valence-band maximum common to all zinc-blende structure III-V compounds, and the six equivalent conduction-band minima near the zone boundary in the [100] directions. Optical absorption therefore requires the absorption or emission of momentum conserving phonons. These processes were examined in detail by Dean and Thomas.[11] The absorption edge consists of a series of steps each associated with the absorption or emission of a particular phonon (at low temperatures, only emission processes are observed). The detailed line shape can be more easily seen using wavelength modulation, so that the first derivative of the absorption is measured. This technique was widely used about ten years ago at low resolution (corresponding to the relatively poor samples then available) for studying indirect excitons under stress in Ge,[15] Si,[15,16] AlSb,[17] and GaP.[18] More recently, high-resolution measurements in the absence of stress on Ge (Ref. 4) and Si (Ref. 6) have yielded detailed absorption line shapes, and simultaneously with the present work, measurements on GaP have been performed.[19] High-resolution measurements on Si at low stresses have also been recently carried out.[8]

In the present work, we have used the wavelength-modulation technique at high resolution in conjunction with stress to examine in detail the anomalous absorption line shape in GaP. The stress-induced splitting of the degenerate valence-band maximum leads to a simplification of the line shape, which permits rather accurate determination of some of the details of the zero-stress exciton dispersion curves. Stress measurements at high resolution also give a more accurate pic-

ture of the effect of stress on the band structure.

In Sec. II, we formulate the extensions to existing theory which are required to fit the splitting pattern of the excitons for the three stress directions considered. Section III describes experimental details, and the main results are summarized in Sec. IV. In Sec. V, we discuss the results under four headings: fine structure, exciton splitting, broadening, and the zero-stress spectrum. The discussion is mainly confined to the results for [001] stress and zero stress, since these are the best understood and therefore, at present, the most informative. We summarize the conclusions of the paper in Sec. VI. In the Appendix we give the generalization of the camel's back $\vec{k}\cdot\vec{p}$ theory[13] to the case where the masses of X_1 and X_3 conduction bands differ. An expression is given for the absorption coefficient due to an exciton with a camel's back dispersion curve.

II. THEORY

The behavior of conduction and valence bands under stress has been fully discussed by several authors,[15,16,19-21] whose results we use. In the present case, we want to take into account the zero-stress splitting of the exciton and (rather approximately) the exciton binding energy as functions of stress, since both are seen to be important experimentally.

Group theory shows that the ground state of an indirect exciton formed from the lowest (X_1) conduction band[22] and highest (Γ_8) valence band of GaP is allowed to split (valley anisotropy splitting):

$$\Gamma_8 \otimes X_1 = X_6 \oplus X_7 \ , \tag{1}$$

where the double group notation is used for the valence band to take account of spin-orbit splitting, and the single group notation for the conduction band, where we assume that spin is unimportant, i.e., we neglect exchange interaction. The valley anisotropy splitting is the result of lifting the degeneracy between $|m_j| = \frac{3}{2}$ and $|m_j| = \frac{1}{2}$ states due to the axial symmetry introduced by the anisotropy of the electron valley (the valley axis is taken as quantization axis).

The variation of the position of exciton lines under stress is dominated by the stress splitting of the valence band and the shift of the conduction band, which are well understood. There will be an additional stress dependence due to the change in binding energy when the valence bands are split. In order to explain the experimentally observed shifts, we need to take this effect into account.

The problem of indirect excitons of this sort has been treated in perturbation theory by Lipari and Baldereschi[1] as an extension of their theory for direct excitons,[23] and with a more accurate variational approach by Lipari and Altarelli.[2] Here we make use of the greater simplicity of the perturbation method (at the expense of quantitative accuracy) to give an estimate of the change in exciton binding energy with stress. The exciton Hamiltonian for the relative motion is given by

$$H_{ex} = H_e(p) - H_h(p,\epsilon) - e^2/\kappa r \ , \tag{2}$$

where $H_e(p) = (p_t^2/2m_t) + (p_l^2/2m_l)$, m_l and m_t being the longitudinal and transverse electron mass (we neglect the camel's back in this calculation), $H_h(p,\epsilon)$ is the 4×4 Hamiltonian describing the degenerate valence-band maximum under stress, and the third term is the Coulomb interaction of electron and hole. p denotes the relative momentum and 2ϵ the stress splitting of the uppermost valence band.

We follow a procedure similar to that of Ref. 1. In Ref. 1 the Hamiltonian is split into two parts, H_s and H_d, which have spherical and d-like symmetry, respectively. Here we split the Hamiltonian into a part H_0 including H_s and the strain terms, and H_d, the nonspherical terms of the unstressed crystal. H_0 is diagonalized by means of the rotation which makes the strain tensor diagonal. H_d is then treated as a perturbation.

For [001] stress, we consider first the exciton formed with the electron in the [001] valley (singlet) and the hole in the fourfold ($m_j = -\frac{3}{2}, -\frac{1}{2}, \frac{1}{2}, \frac{3}{2}$) valence band. For this exciton the Hamiltonian reads

$$H_{ex} = \begin{bmatrix} P+Q_e+Q_h+\epsilon & L & M & 0 \\ L^* & P+Q_e-Q_h-\epsilon & 0 & M \\ M^* & 0 & P+Q_e-Q_h-\epsilon & -L \\ 0 & M^* & -L^* & P+Q_e+Q_h+\epsilon \end{bmatrix} , \tag{3}$$

where

$$P=\frac{p_x^2+p_y^2+p_z^2}{2\mu_0}-\frac{e^2}{\kappa r}\,,\quad Q_{e,h}=\frac{p_x^2+p_y^2-2p_z^2}{2\mu_{1e,h}}\,,$$

$$L=\frac{-i(p_x-ip_y)p_z}{2\mu_{2h}}\,,\quad M=\frac{\sqrt{3}(p_x^2-p_y^2)}{2\mu_{1h}}-\frac{ip_xp_y}{2\mu_{2h}}\,,$$

$$\epsilon=b(s_{11}-s_{12})X\,,$$

and

$$\frac{1}{\mu_0}=\frac{1}{3}\left(\frac{2}{m_t}+\frac{1}{m_l}\right)+\frac{\gamma_1}{m_0}\,,\quad \frac{1}{\mu_{1e}}=\frac{1}{3}\left(\frac{1}{m_t}-\frac{1}{m_l}\right),$$

$$\frac{1}{\mu_{1h}}=\frac{\gamma_2}{m_0}\,,\quad \frac{1}{\mu_{2h}}=\frac{2\sqrt{3}\gamma_3}{m_0}\,.$$

γ_i are the Luttinger valence-band parameters. Terms in P and ϵ are taken as H_0, whose solutions are two doubly degenerate hydrogenic series with a Rydberg of

$$R_0=\mu_0 e^4/2\hbar^2\kappa^2\,, \tag{4}$$

and split by 2ϵ from each other. These states can be classified by orbital angular momentum quantum number l and m. The exciton ground states ($l=0$) are coupled by H_d to d-like excited states ($l=2$): by Q to states with $m=0$, by L to states with $|m|=1$ and by M to states with $|m|=2$.

The only terms which can interfere in Eq. (3) therefore are those in Q_e and Q_h, which gives rise to the valley-anisotropy splitting. Each term of H_d, treated in second-order perturbation theory, gives rise to an infinite sum of squared matrix elements divided by energy denominators. These sums are tabulated[23,24] for a range of splittings δ of the hydrogenic series involved as the function $S_1(\delta)$. The terms in Q in Eq. (3) are strain independent, as they give rise only to intraseries coupling. The terms in L and M, however, are changed by the strain due to the change in energy denominators, and are proportional to $S_1(\delta)$. The solution of the perturbation secular determinant for a stress along [001] is given at the top of Table I in the columns headed δE_B and δE_{ex} which give the change in binding energy and in exciton splitting, respectively. It is important to note that the X_6 and X_7 excitons are not mixed by stress in this case, since the stress direction is parallel to the valley axis. For the doublet excitons under [001] stress (i.e., the electron is in the [100] or in the [010] valley) the Hamiltonian becomes

TABLE I. Shift and splitting of excitons under uniaxial stress.

Stress direction	Valley	Part of exciton binding energy due to H_d δE_B	Exciton splitting δE_{ex}	Conduction-band shift δE_{cb}	Hydrostatic δE_H
[001]	[001]		$-\epsilon_+ \mp (\epsilon_- - D)$	$\frac{2}{3}\zeta$	
	[100], [010]	$(A+B)+(B+C)R(\pm\delta)$	$-\epsilon_+ \mp [(\epsilon_- + \frac{1}{2}D)^2 + \frac{3}{4}D^2R(\pm\delta)]^{1/2}$	$\frac{1}{3}\zeta$	η
	[001]	$A+(\alpha-\beta)^2B+\frac{4}{3}\alpha\beta C$	$-\epsilon_+ \mp \{(\epsilon_- + (\alpha-\beta)D]^2 + 4\alpha\beta D^2R(\pm\delta)\}^{1/2}$	$\frac{1}{3}\zeta$	
[110]	[100], [010]	$+\{(1+4\alpha\beta)B+[\frac{2}{3}+\frac{1}{3}(\alpha-\beta)]^2C\}R(\pm\delta)$	$-\epsilon_+ \mp \{[\epsilon_- - \frac{1}{2}(\alpha-\beta)D]^2 + (\frac{3}{4}+\alpha\beta)D^2R(\pm\delta)\}^{1/2}$	$\frac{1}{6}\zeta$	η
[111]	all	$(A+\frac{1}{3}C)+(2B+\frac{2}{3}C)R(\pm\delta)$	$-\epsilon_+ \mp [\epsilon_-^2 + D^2R(\pm\delta)]^{1/2}$	0	η

Where[a] $A=\frac{16}{5}(\mu_0/\mu_{1e})^2S_1(0)$, $B=\frac{16}{5}(\mu_0/\mu_{1h})^2S_1(0)$, $C=\frac{4}{5}(\mu_0/\mu_2)^2S_1(0)$, $D=\frac{32}{5}(\mu_0^2/\mu_{1e}\mu_{1h})S_1(0)$, $\delta=\epsilon_1-\epsilon_2$, $\epsilon_\pm=\frac{1}{2}(\epsilon_1\pm\epsilon_2)$, $R(\pm\delta)=S_1(\pm\delta)/S_1(0)$, $\zeta=\mathcal{S}_2(S_{11}-S_{12})X$, $\eta=(\mathcal{S}_1-a)(S_{11}+2S_{12})X$, $\alpha=\frac{1}{2}+[1/(4+\gamma^2)]^{1/2}$, $\beta=\frac{1}{2}-[1/(4+\gamma^2)]^{1/2}$, where $\gamma=dS_{44}/b(S_{11}-S_{12})$.

[a] ϵ_1, ϵ_2 are the valence-band shifts for the $|\frac{1}{2}\rangle$ and $|\frac{3}{2}\rangle$ bands, respectively. The upper sign of $\pm$ signs refers to the $|\frac{1}{2}\rangle$ band and the lower to the $|\frac{3}{2}\rangle$ band. X is negative for compression.

$$H_{ex}=\begin{bmatrix} P+Q_e+A+\epsilon & L & B & 0 \\ L^* & P+Q_e-A-\epsilon & 0 & B \\ B^* & 0 & P+Q_e-A-\epsilon & -L \\ 0 & B^* & -L^* & P+Q_e+A+\epsilon \end{bmatrix},$$

where $A=\frac{1}{2}Q_h+\frac{1}{4}\sqrt{3}(M+M^*)$, $B=-\frac{1}{2}\sqrt{3}Q_h+\frac{1}{4}(3M-M^*)$.

The perturbation secular determinant is no longer diagonal due to terms in Q coupling the $|\frac{3}{2}\rangle$ and $|\frac{1}{2}\rangle$ exciton ground states (similar terms in M cancel). This corresponds to the valley-anisotropy splitting not being diagonal under stress, and the X_6 and X_7 excitons are mixed. The solution of the perturbation secular determinant given in Table I shows this point clearly. (D is half the valley anisotropy splitting). The remaining entries in Table I have been calculated in a similar way to the above cases, and we do not give the derivation in detail.

We have ignored in the above contributions to the exciton binding energy variation arising from the spin-orbit split off band. This is a good approximation, as the energy denominators do not vary by much. There is, however, an observable change in the stress dependence of the $|\frac{1}{2}\rangle$ valence band due to this coupling, and we include this by modifying the quantities in the above:

$$\epsilon_1=\tfrac{1}{2}(\zeta-\Delta)+[\tfrac{1}{4}(\Delta+\zeta)^2+2\zeta^2]^{1/2},\quad \epsilon_2=-\zeta\ ,$$

where

$$\zeta=b(S_{11}-S_{12})X \text{ for } \vec{X}\parallel[001],$$

$$\zeta=dS_{44}X/2\sqrt{3} \text{ for } \vec{X}\parallel[111],$$

and a more complicated expression which we do not quote for $\vec{X}\parallel[110]$.[21]

The results of this procedure are: (a) The valley-anisotropy splitting is in general not diagonal giving rise to nonlinear effects in the low-stress region. Since perturbation theory is known to be inadequate for predicting the valley-ansiotropy splitting, we have used experimental values to determine D in fitting the deformation potentials. (b) The exciton binding energies change little for excitons associated with the $|m_j|=\frac{1}{2}$ valence band (which shifts to higher energy under compressive stress), as the energy denominators increase. Excitons formed from the $|m_j|=\frac{3}{2}$ valence band show much larger nonlinear effects as the energy denominators decrease, and ultimately as they cross the excited states of the $|\frac{1}{2}\rangle$ valence-band exciton. In this limit, the perturbation theory ceases to be applicable.

In the region in which perturbation theory applies the exciton energy is given by

$$E_{ex}=E_g-R_0-\delta E_B+\delta E_{ex}+\delta E_{cb}+\delta E_H\ ,$$

where E_g is the band gap in the absence of stress, R_0 is the unperturbed binding energy from the solution of H_s alone. δE_B is the extra binding energy due to H_d without the valley-anisotropy splitting term. The stress-dependent term $(B+C)$ in the expression for δE_B under [001] stress is 1.6 meV; the corresponding terms for [110] and [111] stress are 1.4 meV and 1.3 meV, respectively. δE_{ex} is the splitting of the exciton, including both valence-band and valley-anisotropy splitting, δE_{cb} is the shift of the conduction band, and δE_H the difference between the conduction- and valence-band shifts due to the hydrostatic component of the stress.

If we neglect the changes in the exciton binding energy with stress, the valley anisotropy splitting can still be accounted for by setting $S_1(\delta)=S_1(0)$ in the expressions of Table I. In this approximation, the results for [001] stress reduce to those quoted by Capizzi *et al.*[8] who worked in the low-stress limit. We have neglected in this treatment changes in band parameters with stress; presumably a good approximation for the valence band. As will be seen, this is a poor assumption for the conduction band, and may be a significant omission.

As is well known, and can be seen from Table I, the effect of [001] and [110] stress is to split both conduction- and valence-band degeneracies, while all the conduction bands are equivalent under [111] stress, and only the valence band is split. For [111] stress, therefore, the excitons should split into two, and for [100] and [110] stress, they should split into four components. In general, the center of mass and relative motion of electron and hole cannot be separated due to the valence-band degeneracy.[2] As the latter is removed by stress the exciton problem becomes separable in the high-stress limit. In this case, the total exciton mass depends on the valence band involved and on the orientation of the conduction-band valley axis to the hole mass ellipsoid. We then expect different dispersion relations for the various exci-

TABLE II. This table is identical to Table II of G. E. Pikus, Fiz. Tverd. Tela 19, 1653 (1977) [Sov. Phys. Solid State 19, 965 (1977)] (except for LA↔LO) obtained independently of the intermediate state involved. The letters represent sums of reduced matrix elements corresponding to the following intermediate states: Q, X_5; S, Γ_1; U, X_3; W, Γ_{15}, where the notation is that of Ref. 26.

Transition	LA phonon ∥	LA phonon ⊥	LO phonon ∥	LO phonon ⊥	TA, TO phonon ∥	TA, TO phonon ⊥
$\lvert\frac{1}{2}\rangle \rightarrow z$ singlet	4α	β	0	γ	2η	4θ
$\lvert\frac{3}{2}\rangle \rightarrow z$	0	3β	0	3γ	6η	0
$\lvert\frac{1}{2}\rangle \rightarrow x+y$ doublet	8β	$\alpha+\beta$	2γ	4γ	2θ	$5\eta+\theta$
$\lvert\frac{3}{2}\rangle \rightarrow x+y$	0	$3(\alpha+\beta)$	6γ	0	6θ	$3(\eta+\theta)$
X_6	$4\alpha+2\beta$		2γ		$2\eta+8\Theta$	
X_7	6β		6γ		6η	

$\alpha=\frac{1}{3}(S_{LA}+U_{LA})^2$, $\beta=\frac{1}{3}(S_{LA}+Q_{LA}/\sqrt{2})^2$, $\gamma=\frac{1}{6}(W_{LO}+Q_{LO})^2$, $\eta=\frac{1}{12}(W_T+\sqrt{2}U_T)$, $\theta=\frac{1}{12}(W_T+\sqrt{2}Q_T)^2$.

tons which should show up in the exciton line shapes. A more detailed analysis of the results along these lines will be the subject of a later publication.

The relative intensities for the indirect exciton absorption for the stress-split excitons can be calculated group theoretically for particular phonons and intermediate states, as has previously been done for Si for all phonons,[25] and for AlSb for the LA phonon.[17]

This approach has been extended by Smith and McGill[26] to treat processes with different intermediate states simultaneously for the case of Si at zero stress. We have performed a similar analysis for GaP under [001] stress. Since the method is identical to that of Ref. 26, we do not describe it in detail. The intermediate states considered are Γ_1, Γ_{15}, X_3, and X_5; Γ_{12} and Γ_{25} intermediate states are ignored because of the large energy denominators associated with such processes. The analysis is exact only at the X point, and is therefore only strictly valid for the hump of the camel's back.

We find results identical to those for Si,[26] provided the LA phonon (GaP) is taken to correspond to the LO phonon (Si) and vice versa. The values of the numerical coefficients are different from those of Ref. 26, because we have used unsymmetrized matrix elements. This is purely a matter of definition. The results are given in Table II for [001] stress. Also given are the zero-stress intensities for the two valley-anisotropy split ground states. None of the phonon replicas requires more than two parameters to specify the intensity of all its stress-split components. Since the absolute intensity scale is arbitrary, this means that one free parameter should fit all the relative intensities. For the LO phonon (not observed experimentally), there is not even this freedom, and the relative intensities are fixed by theory.

These results do not include differences in the dispersion relations of the various excitons. In the case of GaP, such differences would have to be taken into account for a quantitative interpretation of the observed strengths. A good check on the self-consistency of any method of measuring experimental relative intensities is the requirement of isotropic absorption at zero stress. This means that (a) the sum of the intensities over valence bands and polarizations ($\parallel+2\perp$) for transitions to the singlet valley should be half the same sum for the doublet valleys, and (b) the sum of the intensities over valence bands and valleys should be the same for all polarizations.

III. EXPERIMENTAL DETAILS

The transmission measurements were made with a Spex $\frac{3}{4}$-m single-grating monochromator, using a vibrating silica plate inside the exit slit modulated at about 12 Hz to produce the wavelength modulation. Modulation amplitude and slit width were approximately equal. Two resolutions were used, the lower with a 5000-Å blaze grating used in first order, and the higher with a 1-μm blaze grating used in second order, corresponding to 0.5- and 0.25-meV resolution, respectively, with a slit width of 0.1 mm. Most of the stress measurements were performed at the higher resolution. The light source was a quartz-halogen lamp. The light was detected with a RCA GaAs cathode

photomultiplier, the signal extracted with a lock-in amplifier, and the output from this was divided by the transmitted light intensity using a ratiometer. This gives a line shape which is proportional to the wavelength derivative of the absorption coefficient: effects of multiple reflections can be shown to be negligible.

The measurements were made with the samples immersed in pumped liquid He. The stress rig was a standard design capable of exerting a force of up to about 40 kg, so that rather thin (0.75×0.75 mm^2) samples had to be used to obtain high stress ($\lesssim 8$ kbar). The samples were mounted between brass caps into which holes were bored which fitted the sample closely, thus ensuring that the sample was mounted vertically, and the holes were filled with indium. The indium becomes sufficiently hard at low temperatures to transmit the forces required, but remains soft enough to ensure uniaxial stress. The linewidth of the spectra was slightly larger at high stress than at low, but the fine structure could still be easily resolved. Measurements in which the lines shift by 100 linewidths set particularly stringent requirements on the uniformity of the stress. The samples used were at least five times longer than their width to minimize end effects, although in practice it was found that the structure was not noticeably broadened even if the whole length of the sample was used for the optical measurements.

The stress samples were cut from Czochralski grown material. Those for [001] and [110] stress directions were doped with S ($n = 5 \times 10^{17}$ cm^{-3}), and those for [111] stress were Te doped ($n = 1 \times 10^{17}$ cm^{-3}).[27] As a check to ensure that the structure studied was intrinsic a relatively high-purity sample[27] grown from Ga solution containing about a factor of 20 less S and a factor of 50 less N (estimated from the strength of the no-phonon absorption lines) was also measured. This sample showed sharper absorption structure, but its size and thickness (~300 μm) precluded stress measurements, and only permitted a reliable high-resolution line shape to be obtained for the strong LA-phonon replica. The two kinds of sample are designated as "doped" and "pure" in the text. The S-doped sample no-phonon nitrogen line (A line) had a peak absorption coefficient of about 10 cm^{-1}, corresponding to a nitrogen concentration of about 2×10^{16} cm^{-3}.

IV. RESULTS

In Fig. 1, the wavelength derivative spectra in the absence of stress are shown for the three free exciton phonon replicas observed. Except for the LA-phonon structure, the spectra for the "doped" sample are presented at both high- and low-resolution to facilitate comparison with the "pure" sample results.

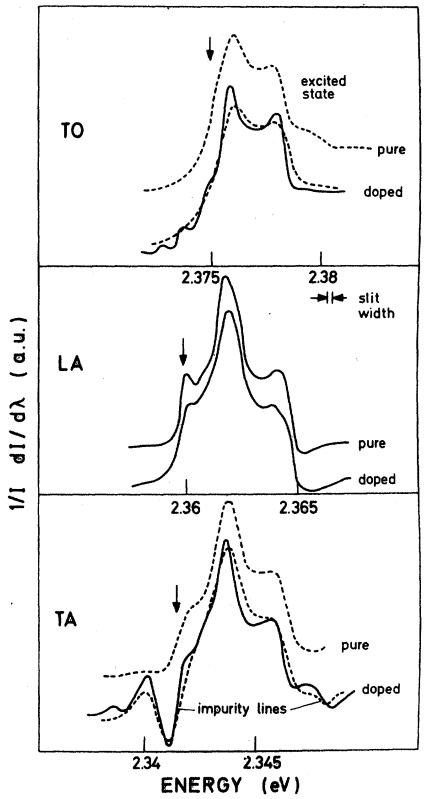

FIG. 1. Normalized wavelength derivative transmission spectra of two samples of GaP without stress. The vertical scale is arbitrary, but about four times larger for the TA and TO replicas than for the LA. The structures are plotted above one another for convenient line-shape comparison. The dashed curves are "low"-resolution spectra, i.e., 0.5-meV slit width. The slit width marked corresponds to "high" resolution (0.25 meV). The absorption thresholds of Ref. 11 are marked with arrows. The energy scales are linear in wavelength, not energy.

The agreement with the results of Dean and Thomas[11] is good; their threshold for each phonon replica is marked by an arrow above the spectrum. The fine structure is clearly seen, and it is somewhat different for the three phonon replicas. The stress measurements clarify this difference, and we return to it later (Sec. VD).

The LA line shape is essentially the same in both high- and low-purity material, although less sharp for the latter. The TA line shape, however, is severely distorted by an impurity line for the doped material (The position of this structure suggests that it is the LA replica of the sulphur line). We thus conclude that the LA-phonon line shape in the doped material is essentially intrin-

sic, while the TA is not. This is a fortunate coincidence, since the LA is the strongest phonon replica, which is therefore the easiest to study experimentally. It is also nondegenerate, which eliminates a possible source of confusion in stress measurements. The TO-phonon replica is essentially the same for both samples, except for an extra structure on the high-energy side for the pure material. This we interpret as the LA-phonon replica of an excited state, as discussed in Sec. V D.

Under [001] stress the LA-phonon replica splits as shown in Fig. 2. Each structure is labeled with the valence and conduction band from which the exciton is formed. The most striking feature is that each exciton has a doublet structure, which immediately indicates the source of the complexity at zero stress. As we shall see later (Sec. V A), this doublet structure can be attributed directly to the presence of a camel's back in the conduction band. The second point to note is that the $|\frac{1}{2}\rangle$-$|\frac{3}{2}\rangle$ splitting of the excitons depends on the conduction band involved, since it is a combined effect of the valley-anisotropy and valence-band splittings. The value of stress chosen for Fig. 2 is such as to minimize the distortion of the spectra by extraneous effects, such as superposition of transitions mediated by phonons other than LA. Even so, this is not entirely successful. The structure at and below 2.35 eV is due to the high-energy component of the TA phonon. The $|\frac{1}{2}\rangle$ singlet exciton is not completely polarized $\vec{E} \parallel \vec{X}$, and the $|\frac{3}{2}\rangle$ singlet exciton is somewhat distorted in consequence, but at stresses where these are resolved the high-energy component of the TA phonon overlaps with the LA structures. There is a similar problem near 2.37 eV, where the minimum on the high-energy side of the $|\frac{3}{2}\rangle$ doublet exciton (which can be seen more clearly in Fig. 10) is obscured by overlap with the $|\frac{1}{2}\rangle$, singlet TO-phonon replica.

The energies of the LA structures observed are plotted as functions of stress in Fig. 3. For these plots we have chosen the energies of the highest point in the peaks. As will be seen in the line-shape treatment of Sec. V A these energies do not represent exactly the critical energies, but provide a simple criterion to represent them. The continuous lines in Fig. 3 are fits using the expressions in Table I. In the region of 4 kbar, the excitons formed from the $|\frac{3}{2}\rangle$ valence band start abruptly to broaden (see Sec. V C). Also in this region, these excitons show curvature as functions of stress which is fitted reasonably well by the calculation of the change in exciton binding energy. The deformation potentials used for the fit are given in Table III.

The results for stresses higher than 4.5 kbar were taken at the lower (0.5 meV) resolution. This was necessary to follow accurately the $|\frac{1}{2}\rangle$

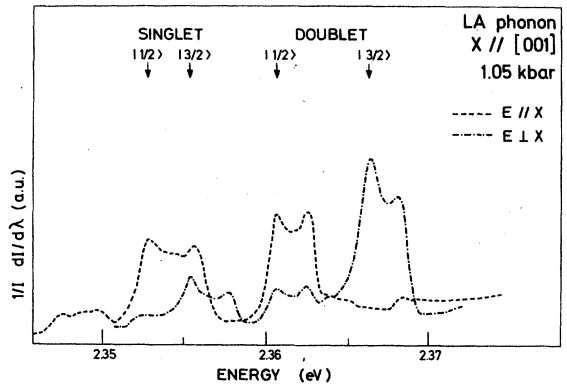

FIG. 2. Normalized wavelength derivative transmission spectra at low [001] stress for the two polarizations. The lower structure of each doublet is marked, and the valence and conduction bands from which the exciton are formed indicated.

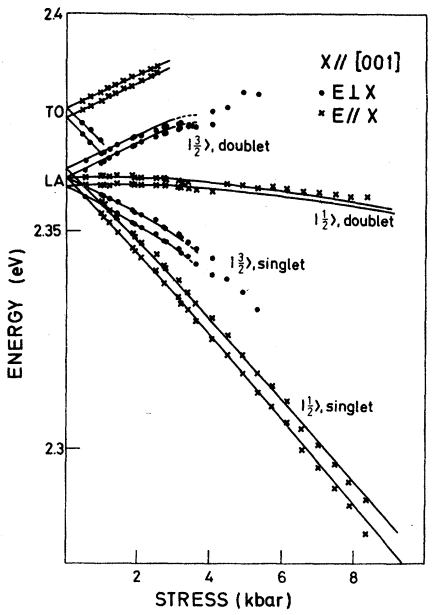

FIG. 3. Exciton splittings as functions of [001] stress. The points correspond to the peaks of the doublets of Fig. 2. The lines are fits using the expressions of Table I (see Sec. II) and the deformation potentials of Table IV, a mean zero-stress binding energy of 19 meV, mean zero-stress exciton energies of 2.3611 and 2.3631 eV, and valley-anisotropy splittings of 2.0 and 2.2 meV for the lower and upper peaks, respectively. The spin-orbit splitting was assumed constant at 0.08 eV. The TO-phonon replica splitting is also shown, with zero-stress energies of 2.3770 and 2.3749 eV. Otherwise the fitting parameters are the same as for the LA replica.

TABLE III. Deformation potentials of GaP (in eV).

Stress direction	This work [001]	This work [110]	This work [111]	Previous work
$\mathcal{E}_2$	6.5, 6.9[a]	5.9, 6.2[a]		6.8[18,b]
b	−1.8	−1.8		−1.4[18,b]
d		−4.9	−4.3	−4.4[18,b]
$\mathcal{E}_1 - a$	1.6	1.6	1.6	−3.7[18,b], 1.0 (Ref. 29)

[a] Where two values are shown, the former refers to the hump of the camel's back, and the latter to the minima.

[b] These values have been corrected using the experimental compliance coefficients which were also used in the present work (Ref. 31).

singlet structure whose width increases and peak height falls with increasing stress (see Sec. V A). This reduction of resolution is responsible for the slight discontinuity in the $|\frac{1}{2}\rangle$ doublet structure in this region.

The split components of the TO-phonon replica are also plotted in Fig. 3. It gives rise to only two excitons that can be followed as functions of stress. They are fitted in the figure with shifted curves of the same shape as those for the LA $|\frac{1}{2}\rangle$ singlet and $|\frac{3}{2}\rangle$ doublet excitons. This simple splitting pattern is a result of the simpler structure of the TO-phonon replica at zero stress, as a consequence of the selection rules of Table II determined by the dominant intermediate state for the process.

Under [110] stress, the splitting is similar (Fig. 4). The structures are all doublets, with the exception of the $|\frac{1}{2}\rangle$ doublet exciton which has a clearly defined extra peak on its low-energy side. This persists over the range of stresses studied (less for [110] stress than for the other two stress directions). The splitting pattern is plotted in Fig. 5, and fitted to expressions from Table I. The dashed curve follows the extra structure with stress, and was constructed by eliminating the curvature due to valley-anisotropy splitting. It can be seen to fit rather well the lowest energy peak of the doublet exciton and to merge with the lower component of the doublet at zero stress. This is an experimental observation, which we cannot justify theoretically.

The [111] stress results show marked qualitative changes of line shape with stress (Fig. 6). There is an extra structure on the low-energy side of the $|\frac{1}{2}\rangle$ exciton (the conduction bands are equivalent) as for [110] stress, and a second one appears

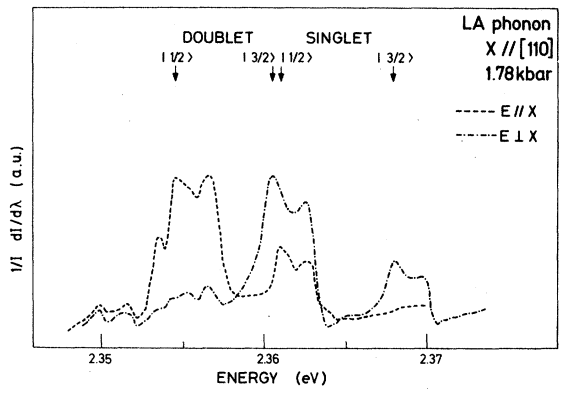

FIG. 4. Normalized wavelength derivative transmission spectra for [110] stress. The comments of Fig. 2 apply.

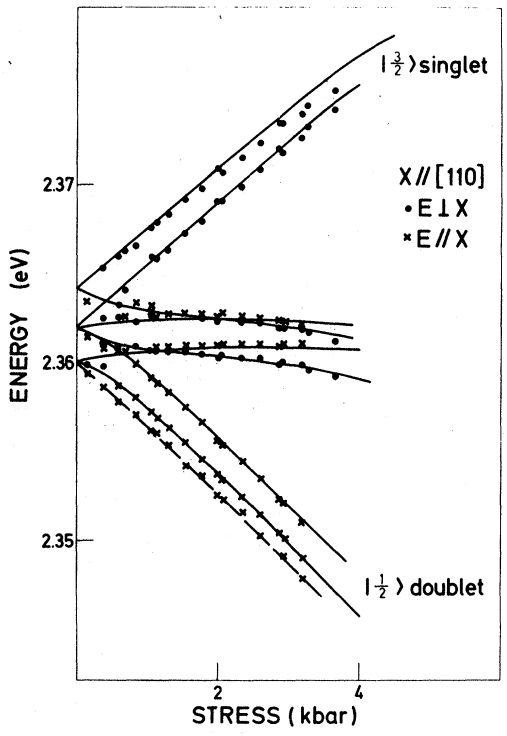

FIG. 5. Exciton splittings as functions of [110] stress. The comments of Fig. 3 apply. The dashed line is constructed as described in the text with the equations of Table I.

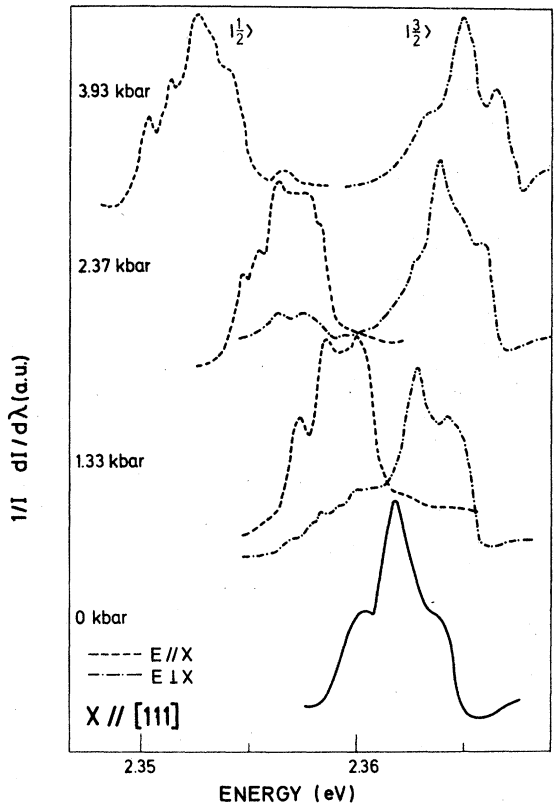

FIG. 6. Normalized wavelength derivative transmission spectra for three different stresses along [111], with a zero-stress spectrum for comparison.

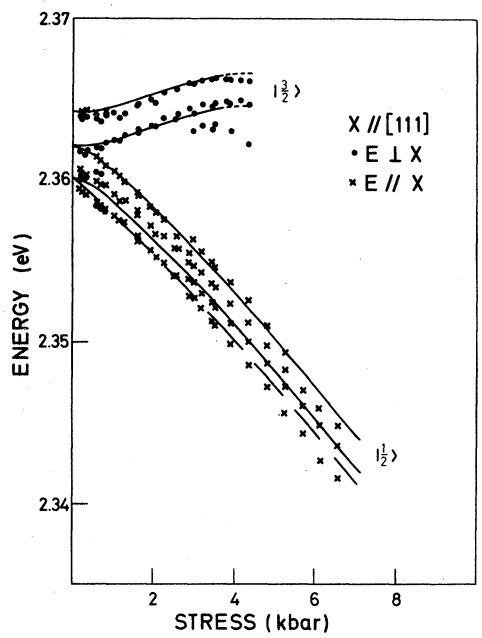

FIG. 7. Plot of the peaks (or shoulders) observed under [111] stress as functions of stress. The comments of Fig. 3 apply. The dashed line is constructed as described in the text.

at higher stress. The $|\frac{3}{2}\rangle$ exciton shows continuous line-shape changes which we attempt to represent with the three spectra of Fig. 6. Peaks or shoulders are plotted in Fig. 7 as functions of stress. The complexity of the structure is such that only the overall behavior could be said to be expected. The solid curves were thus obtained with the expressions of Table I with the deformation potentials adjusted to follow the general trend of the points (see Table III). The extra (dashed) line has been constructed in the same way as that for [110] stress, and with as little justification. It should be noted that because of the complexity of the spectra systematic errors can give rise to a larger scatter of points than for the other stress directions.

V. DISCUSSION

A. Fine structure

The first point we consider is the peculiar doublet structure of the excitons under stress, which is clearly responsible for the complexity of the zero-stress spectrum. For an indirect exciton formed from a parabolic conduction band and nondegenerate valence band (such as we might expect to have under stress), the absorption coefficient is expected to vary as the square root of the energy above threshold[28] giving rise to an inverse square-root singularity in the derivative, or, in the experimental spectrum, a single asymmetric peak near the threshold. The doublet structure suggests a second singularity in the derivative of the density of states. Since the electron mass parallel to the valley axis is very much larger than the hole mass, it is to be expected that the exciton dispersion curve should approximate to that of the electron in this direction. A camel's back structure in the conduction band should therefore give rise to a similar structure in the excited dispersion curve. This conclusion is borne out by the calculation of Ref. 3, which includes a camel's back.

Of the different excitons studied, the $|\frac{1}{2}\rangle$ singlet exciton is expected to have a dispersion parallel to the valley axis which approximates most closely to that of the conduction band, since the $|\frac{1}{2}\rangle$ valence band has a light hole mass parallel to the valley axis.[20] In Fig. 8, we show a fit to the experimental line shape of this exciton using the expression given in the Appendix for the absorption. We take the quality of the fit as strong evidence that the fine structure is indeed due to a camel's

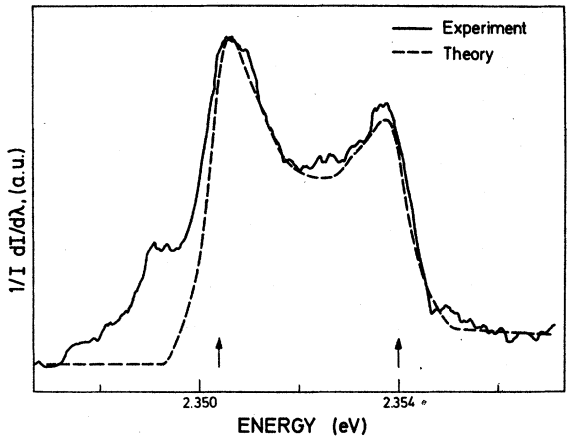

FIG. 8. Fit using Eq. (A6) to the $|\frac{1}{2}\rangle$ singlet exciton line shape under [001] stress at 1.032 kbar, using $\Delta = 346$ meV, $\Delta_0 = 424.2$ meV, exciton energy at camel's back peak = 2.3540 eV, Lorentzian linewidth = 0.7 meV. The parameters give a camel's back height of 3.61 meV. The extra structure on the low-energy side is the TA-phonon $|\frac{3}{2}\rangle$ doublet exciton. Arrows mark the positions of the singularities from the fit.

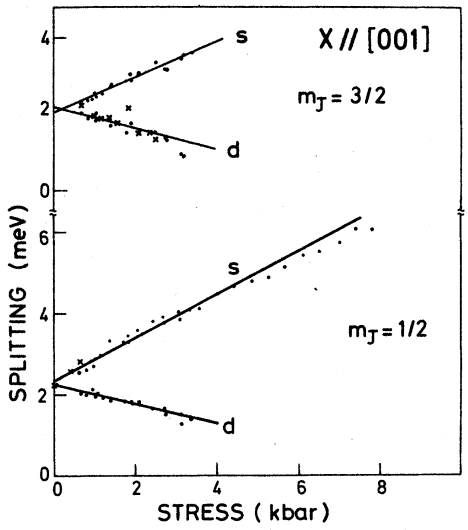

FIG. 9. Splitting of the doublet structures observed for the four excitons under [001] stress. The peak energies are plotted, although they do not correspond exactly to the camel's back extrema. The straight lines are least-squares fits to the LA-phonon data. The slopes are 0.53 meV/kbar, ($|\frac{1}{2}\rangle$, singlet), 0.43 meV/kbar ($|\frac{3}{2}\rangle$, singlet), -0.24 meV/kbar ($|\frac{1}{2}\rangle$, doublet), and -0.27 meV/kbar ($|\frac{3}{2}\rangle$, doublet) with intercepts with zero stress of 2.35, 1.93, 2.23, and 2.06 meV, respectively. The measurements at stresses above 4.5 kbar were performed at lower resolution, which reduces the peak separation measured. This has been compensated for by shifting the corresponding points, so that high- and low-resolution measurements near 4.5 kbar agree. Crosses mark points from the TO-phonon replica.

back, whose height is given rather accurately by the fit. This height is that of the exciton, which is expected to be somewhat less than that of the conduction band. A more sophisticated analysis of the differences in line shape of the various excitons will be the subject of a future publication.

Having identified the doublet structure as due to a camel's back in the exciton dispersion curve, we now turn to its stress dependence. The doublet splittings of the four excitons seen for [001] stress are plotted in Fig. 9. These are actually peak splittings, which, as shown by the vertical arrows in Fig. 8 differ slightly from those of the singularities; however, the trends should be approximately correct. The changes of the splittings with stress are linear within experimental error, with an increasing camel's back for the singlet exciton, and a decreasing one (which can no longer be observed above about 3·5 kbar) for the doublet exciton. The most likely cause for this effect is a change under stress in Δ or P to which the camel's back height [see Eq. (A4)] is very sensitive. We have attempted to estimate the magnitude and sign of this effect with a simple pseudopotential calculation. The results show that the order of magnitude and sign of the change are consistent with this explanation.

The slopes of the lines in Fig. 9 are in approximately the ratio 2 : 1 for the singlet and doublet valleys as expected if the hydrostatic coefficient is small. It is known to be less than 10^{-6} eV/kbar for the X_1-X_3 gap of GaP from infrared absorption measurements.[29] The importance of exciton formation is shown by the different slopes for the two excitons formed from the singlet conduction band.

The crosses in Fig. 9 are points derived from the TO-phonon replica, and are in excellent agreement with those from the LA phonon. This indicates that phonon dispersion, which could only be significant for the LA phonon, is not important. If accurate data on the phonon dispersion were known, this would set an upper limit on k_0, which is the distance of the conduction-band minimum from the X point (see Appendix). An attempt to do this using the neutron scattering results of Ref. 30 gives the estimate that for $k_0 = 0.1 \times 2\pi/a$ the camel's back should appear to be 0.3 meV larger for the LA replica than the TO. This is of course within the limits of experimental error in the neutron measurements, and also comparable to the scatter in the present results. However, we suggest that k_0 is probably not much larger than this value.

B. Exciton splitting

We now turn to the splitting of the excitons observed, and the deformation potentials calculated from them. The fits in Figs. 3, 5, and 7 show nonlinearities due to the valley-anisotropy splitting in the low-stress region (except for the singlet valley under [001] stress). Since the camel's back height is comparable to the valley-anisotropy splitting, it is difficult to make accurate measurements in this region for some of the excitons, although even in these cases the energy to which the linear part of the curve extrapolates at zero stress provides convincing proof that such effects occur. The stress dependence of the exciton energies confirms the predicted sign of the valley-anisotropy splitting.

Both experiment and theory show nonlinearities in the region of 3–4 kbar for excitons associated with the $|\frac{3}{2}\rangle$ valence band. This we attribute to changes in exciton binding energy as the excitons approach the excited states of the excitons formed from the $|\frac{1}{2}\rangle$ valence band, as discussed in Sec. II. The theoretical fits are satisfactory, even though perturbation theory in this region is suspect.

At high stress (8 kbar), the nonlinearities in the curves are due to coupling with the spin-orbit split off valence band, and are fitted by the theory. The deformation potentials used for the fit are shown in Table III.[31] Even though different conduction-band deformation potentials ($\mathcal{E}_2$) were used for the two extrema of the camel's back, it was not possible to fit the [001] and [110] results with the same values. The difficulty may be caused by the inadequate treatment of the exciton binding energy with stress, which, in particular, does not consider the effect of the camel's back and its variation with stress. In view of our poor understanding of the line shape for the other stress directions, the values of d obtained may be said to agree within experimental error.

The agreement with the results of Balslev[18] is good except for the hydrostatic deformation potential, which we find to be much closer to the value obtained from hydrostatic measurements.[29] The results for [110] and [111] stress are not understood at present. The appearance of an extra structure on the low-energy side of the $|\frac{1}{2}\rangle$ doublet exciton for [110] stress, and a similar one for the [111] stress, is an unsolved problem. It has all the appearance of an exciton splitting effect, in that it can be observed down to the lowest stress. The line-shape changes for [111] stress are, in qualitative terms, to be expected, since the excitons are formed from valence bands which, in the high stress limit, have ellipsoidal constant energy surfaces whose axes are oblique to those of the conduction band. Quantitatively, however, the problem is complex, and requires proper density of states calculations to solve it.

It is worth noting that an extra structure appears for both $|\frac{1}{2}\rangle$ and $|\frac{3}{2}\rangle$ excitons for [111] stress at about the same stress, near 2.8 kbar, although the effect is a gradual development in the line shape, and not abrupt. The possibility that the extra structures are associated with impurities should be considered. Any considerations along these lines are unable to explain why no anomalous structure (apart from that due to the camel's back) appears for the [001] stress direction, while it does for [110] stress, for which samples were cut from the same slice. It is also implausible that sharp impurity lines strong enough to be responsible for the observed structure could be superimposed on the zero stress spectrum without severely distorting it, as observed for the TA-phonon replica.

Attempts to make quantitative comparisons between the predictions of Table II and the experimental relative intensities determined in a simple way lead to results which are not self-consistent, presumably due to the different line shapes and camel's back heights for the different excitons. Nevertheless, it is possible to say that for the LA phonon $\alpha > \beta$ (see Table II), and we estimate the ratio α/β at about 1.6. The Γ_1 intermediate state alone gives $\alpha = \beta$; this observation implies constructive interference between Γ_1 and X_3 processes and/or destructive interference between Γ_1 and X_5 processes.

The TO-phonon replica splits under stress in a way that shows that it is almost entirely the shallower (X_6) state at zero stress. Such a splitting pattern would be impossible for the LO-phonon replica, confirming that it is indeed the TO that is observed, with $\theta \gg \eta$. This implies either nearly total destructive interference between Γ_{15} and X_3 processes or dominance of the X_5 process. The relative intensities observed are approximately consistent with this assignment except that the $|\frac{1}{2}\rangle$ doublet exciton might be expected to be observed for $\vec{E} \parallel \vec{x}$.

No stress measurements were made on the TA-phonon replica. It is clear, however, that the line shape is significantly different from that of the TO at zero stress, showing that different matrix elements are involved, although the two phonons have the same symmetry.

C. Broadening

We have already discussed briefly the nonlinear stress dependence of the energies of the excitons formed from the $|\frac{3}{2}\rangle$ valence band in the region of 3–4 kbar. At higher stresses these excitons are

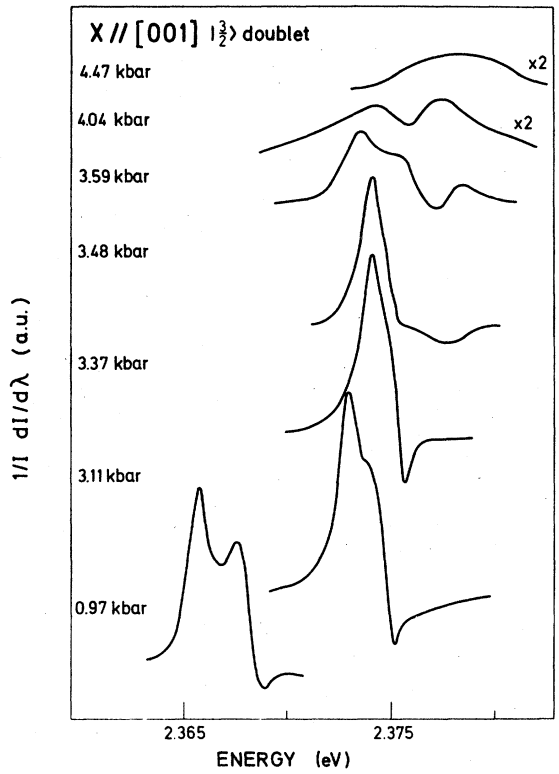

FIG. 10. Line shape of the $|\frac{3}{2}\rangle$, doublet exciton at various stresses, showing the disappearance of the camel's back and the abrupt onset of broadening. Note also the sharp minimum on the high-energy side of the line, which becomes sharper and deeper as the stress increases. Values of stress are given to three significant figures. Absolute accuracy is only of the order of 2%, but the relative precision is higher.

observed to broaden until they become unobservable in the region 5–6 kbar. We attribute both broadening and nonlinearity to similar causes, i.e., the crossing of $|\frac{3}{2}\rangle$ exciton with excited states of the $|\frac{1}{2}\rangle$ exciton formed from the same conduction band. The low-resolution results for Ge (Ref. 15) and Si (Refs. 15 and 16) show similar broadening which occurs at much lower stress in Ge, a fact consistent with the smaller binding energy. The threshold for the broadening is abrupt and can be specified quite accurately. Figure 10 shows an example for the $|\frac{3}{2}\rangle$ doublet exciton under [001] stress, where the spectrum at 3.37 kbar is unbroadened, while that at 3.48 kbar no longer shows the minimum on the high-energy side, and at higher stresses continues to broaden. Similar broadening, starting on the low-energy side in this case, is observed for the $|\frac{3}{2}\rangle$, singlet exciton starting at 4.2 kbar.

Excited states of the excitons are not observed in the doped material used for the stress measurements. We attribute the relatively abrupt onset of broadening to mixing of the $n=1$, $|\frac{3}{2}\rangle$ excitons with the quasicontinuum of excited states of the $|\frac{1}{2}\rangle$ exciton associated with the same conduction band. Broadening is first observed for both doublet and singlet $|\frac{3}{2}\rangle$ excitons when they are separated from the $|\frac{1}{2}\rangle$ ground states by 15.0 ± 0.5 meV. We take this to be close to the energy at which they cross the first excited state. This has a binding energy of about 5 meV according to Ref. 2, so that we estimate the ground-state exciton binding energy at about 20 meV in this way, in good agreement with the result obtained in the next section from the energy of the excited state observed in the pure material at zero stress.

D. Zero-stress exciton parameters

We now return to the results at zero stress, and discuss them in the light of the results of the stress measurements.

The splitting of the TO-phonon replica under stress into only $|\frac{3}{2}\rangle$ doublet and $|\frac{1}{2}\rangle$ singlet excitons (Fig. 3) identifies it as being predominantly due to the upper (X_6) exciton. The extra structure on its high-energy side in the pure material (Fig. 1) cannot then be part of the TO-phonon replica line shape. This structure is totally absent in the impure material, while it is even sharper in the experimental curve shown in Ref. 3. Judging by the clearer structure for the LA replica, the samples used for these measurements were higher quality than those used in the present work. The strong sample dependence of this structure rules out an assignment as the LO-phonon replica, and its appearance only in material of higher purity suggests that it is not due to impurities. It is therefore attributed to the LA-phonon replica of an excited state, and we assign it tentatively to the camel's back peak of the shallower of the valley-anisotropy split $n=2$ s states. This has been calculated in Ref. 2 to have a binding energy of 4.6 meV (in the more precise nomenclature of Ref. 2 this is the first excited X_6 state with even L). The exciton binding energy is then the sum of the excited-state binding energy and the separation between excited and ground states. The excited state is about 15 meV above the LA camel's back peak of the X_6 state, leading to binding energies of 19.5 and 21.5 meV, respectively, for the X_6 and X_7 ground states, and a band gap of 2.3500 eV, using the value of E_{gx} from Ref. 11.

Experimental values for the exciton binding energy in the literature vary between 10 meV (Ref. 11) and 21 meV (Ref. 14), and are summarized in Table IV. Theoretical values favor the higher end of the range of experimental results, with some uncertainty due to the different band parameters

TABLE IV. Exciton parameters for GaP.

	This work	Previous work: Theory	Previous work: Experiment
Binding energy (meV)			
	19.5 (X_6)	17, 19[a]	10[b]
	21.5 (X_7)	17.9, 18.8[c] (dip)	13.8[d]
		18.3, 19.7[c] (hump)	13[e]
		20.5[g]	19[f]
			21[g]
Valley-anisotropy splitting (meV)			
	1.9 (dip)	2[a]	0.9[h](dip)
		0.9[c] (dip)	2.3[h](hump)
	2.3 (hump)	1.4[c] (hump)	
Exciton camel's back height (meV)			
	2.4 (X_7)	3.0 (X_7)[c]	2.5 (X_7)[h]
	2.8 (X_6)	3.4 (X_6)[c]	3.9 (X_6)[h]
$k_0(2\pi/a)$	0.07–0.1		0.047[i]
			0.08[g]

[a] Reference 2.
[b] Reference 11.
[c] Reference 3.
[d] Reference 32.
[e] D. Auvergne, P. Merle, and N. Mathieu, Phys. Rev. B **12**, 1371 (1977).
[f] M. D. Sturge, A. T. Vink, and F. P. J. Kuijpers, Appl. Phys. Lett. **32**, 49 (1978).
[g] Reference 14.
[h] Reference 19.
[i] Reference 12.

and dielectric constant which can be chosen. The most recent calculation,[3] which includes a camel's back and uses recent band parameters, gives a mean binding energy of 18.3 meV at the minima of the camel's back, in reasonable agreement with our results.

Because of the overlap of the X_6 and X_7 exciton line shapes, the zero-stress spectrum of the LA-phonon replica can give directly reliable estimates only for the energies of the high- and low-energy peaks, whose separation is measured as 4.2 meV. This should be the sum of the camel's back and valley-anisotropy splittings, so that we infer from the extrapolation of Fig. 9 to zero stress for the singlet excitons, a valley-anisotropy splitting of 2.3 meV at the hump, and 1.9 meV at the dip. Linear extrapolation of the singlet exciton energies under [001] stress to zero stress (see Fig. 3) gives 2.2 (dip) and 2.4 meV (hump), but this is not as accurate as might be hoped due to the relatively large stress required to resolve the camel's back structures, which is much larger than that required in Si (Ref. 8) where an accurate value was found.

The stress measurements also indicate that the relative intensities of X_6 and X_7 excitons are not equal, as would happen if the Γ_1 conduction band were the only intermediate state: the ratio $X_6 : X_7$ is about 1 : 0.7. This was determined by measuring the area under the peaks at low [001] stress, and assuming that the difference in the shapes of the two structures is not important.

With these parameters in mind we have performed a fit to the zero-stress spectrum of the pure sample. The result is shown in Fig. 11. Although the fit is not perfect, it is good enough to yield meaningful parameters. The different camel's back heights for X_6 and X_7 excitons were obtained (rather artificially) by adjusting Δ in the Lawaetz expression.[13] The minimum on the high-energy side of the experimental curve can never be fitted by an expression of the form we are using, which cannot be made to cutoff sufficiently sharply. This may be the source of some of the deficiencies of the fit.

To obtain the fit we have used camel's back heights which differ by 0.4 meV for the X_6 and X_7 excitons and valley-anisotropy splittings of 2.1 and 1.7 meV for the hump and dip of the camel's back, respectively. The fitting parameters are consistent with those inferred from the stress measurements since for neither method would we claim an accuracy better than 0.2 meV. In view of the possible sensitivity of the fitting parameters to the deficiencies of the fit, we prefer to take the energies of the high- and low-energy peaks

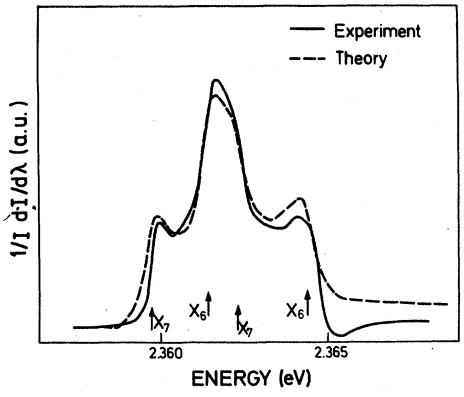

FIG. 11. Fit to the zero-stress spectrum of the "pure" sample using Eq. (A6). The parameters used were $\Delta_0 = 424.2$ meV and X_7 exciton energy at the peak of the camel's back of 2.3623 eV, valley-anisotropy splitting of 2.1 meV at the peak of the camel's back. Lorentzian linewidth of 0.6 meV, and $\Delta = 358$ meV and 353 meV for the X_7 and X_6 excitons, respectively. These parameters give camel's back heights of 2.59 and 2.99 meV for the X_7 and X_6 excitons, respectively. The X_7 exciton was taken to have 0.7 of the oscillator strength of the X_6 exciton. Arrows mark positions of the singularities determined from the fit.

from the fit, but to use valley-anisotropy splittings determined as described above from the extrapolation of Fig. 9, which gives camel's back heights of 2.8 and 2.4 meV for the X_6 and X_7 excitons, respectively, with valley-anisotropy splittings of 2.3 and 1.9 meV at the hump and dip of the dispersion curve. The broadening used was Lorentzian with a width of 0.6 meV, which suggests that instrumental and sample broadening contribute about equally to the linewidth.

The valley-anisotropy splitting in GaP has not to our knowledge been measured before, with the exception of an attempt to deduce it directly from the zero-stress spectrum, giving a value of 0.9 meV.[19] The theoretical values of 0.9 meV (dip) and 1.4 (hump)[3] are about a factor of 2 lower than those we find here. Since a camel's back is included in the calculation, it is difficult to see where the discrepancy can arise, although an unrealistically small Δ (33 meV) was used in order to match Δ, k_0, ΔE, and m_l. The perturbation expression[1] for the exciton binding energies (neglecting camel's back effects) shows that the valley-anisotropy splitting is proportional to $\gamma_2 R_0/\mu_{1e}$ (these parameters are defined in Sec. II). μ_{1e} is dominated by the transverse electron mass m_t which is accurately known from cyclotron resonance,[32] and certainly could not be adjusted by a factor of 2. This suggests that either the theory with a camel's back[3] is inadequate or that γ_2 is significantly larger than the best recent determination.[33] We note that many experiments give linear combinations of the Luttinger parameters (the μ and δ of Ref. 2), which are relatively insensitive to γ_2 since it is comparatively small. The valley-anisotropy splitting should give a more direct measure of this quantity provided the theory is accurate.

Other values in the literature for the camel's back height have been obtained indirectly. Kopylov and Pikhtin[14] found $\Delta E = 3$ meV from an analysis of the energies of excited states of donors, in excellent agreement with our results. An estimate of ΔE can also be obtained from Dean and Herbert's value for k_0 of $0.047(2\pi/a)$ with the aid of the $\vec{k}\cdot\vec{p}$ theory. Taking m=free-electron mass, $\mu = \infty$ and $\Delta = 355$ meV[34] in Eq. (A5) gives $\Delta E = 0.36$ meV, which is incompatible with our results. A value of k_0 about a factor of two larger is needed to give $\Delta E = 3$ meV for reasonable mass parameters.

The result of Ref. 3 that the exciton camel's back heights are 3.4 (X_6) and 3.0 (X_7) meV is based on an attempt to fit both LA- and TO-phonon replicas with the same line shape, i.e., without taking into account the different oscillator strength of the X_6 and X_7 states in the two cases. The structure we assign to the LA-phonon replica of an excited state was treated as part of the TO line shape. The result is nevertheless useful in that it gives an estimate of the relation between the exciton camel's back height and that of the conduction band.

Since no measurements were performed above He temperature, phonon absorption processes were not observed, and the no-phonon exciton energy could not be determined. The excellent agreement found with the results of Ref. 11, however, suggests, that it ould be difficult to improve on them, with the exception of the TO-phonon replica. From our measurements we would place the threshold, defined in a manner consistent with Ref. 11, at 2.3762 eV. For the other phonon replicas, the threshold is determined by the X_7 exciton, while this value corresponds to the X_6. To be consistent with the others it should be reduced by the valley-anisotropy splitting to 2.3743 eV: the TO-phonon energy is then estimated at 45.6 meV, in close agreement with the value 45.3 meV from bound exciton luminescence.[35] A similar correction might be necessary for free exciton luminescence measurements. This may account for the difference between our result and the 44.6 meV found by Mobsby *et al.*[36]

CONCLUSION

We have studied the indirect exciton in GaP under uniaxial stress, using the technique of high-reso-

lution wavelength-modulated absorption. The use of a high resolution yields results on the details of the exciton fine structure and its stress dependence. In particular, we have determined the valley-anisotropy splitting of the exciton ground state and the height of the camel's back in the exciton dispersion curve rather accurately.

A value of the exciton binding energy has been determined from the observation of an excited state at zero stress; level-crossing effects in the stress measurements are consistent with the results so obtained. Effects of the variation of exciton binding energy with stress have also been observed.

The deformation potentials are consistent with those previously obtained, and the discrepancy between the results of uniaxial and hydrostatic pressure measurements is found to be the result of the neglect of the stress dependence of the exciton binding energy and the valley-anisotropy splitting on the uniaxial measurements.

It has been found that the proposed value of k_0 (Ref. 12) is inconsistent with the observed camel's back height and existing theory, and the only obvious deficiency of the theory (except for the assumptions inherent in $\vec{k}\cdot\vec{p}$ perturbation theory) is shown to be unable to account for the discrepancy. By contrast, our result is in excellent agreement with that obtained from fitting the energies of donor excited states.[14] In interpreting the results, we have made use almost exclusively of the [001] stress and zero-stress data, since the results for other stress directions are not understood.

The camel's back height which we have measured is that of the exciton. The results of Ref. 3 suggests that the conduction-band camel's back is of the order of 0.5 meV larger. Even within this error margin, the determination of the camel's back height sets a very stringent requirement on the band parameters, due to its extreme sensitivity to the X_1-X_3 splitting and the matrix element between these bands.

ACKNOWLEDGMENTS

We are most grateful to E. G. Schönherr and E. Winkler for providing the high-purity GaP samples; to G. Poiblaud of R.T.C., Caen and W. Heywang of Siemens for the material used for the stress measurements; to P. E. Simmonds, W. Senske, M. S. Skolnick, and D. Bimberg for helpful discussions; to H. Hirt for technical assistance; and to G. Fröhlich for smaple preparation. One of us (R. G. H.) is grateful to the Royal Society for financial support.

APPENDIX

The $\vec{k}\cdot\vec{p}$ theory suggested by Lawaetz,[13] which treats GaP as a perturbation on Si, is useful to give a clear picture of the origin of the camel's back in GaP. However, the assumption that coupling with other bands due to the antisymmetric potential in GaP is negligible is quantitatively doubtful.

In this Appendix, we generalize the $\vec{k}\cdot\vec{p}$ theory of Lawaetz to eliminate this difficulty, while retaining the simple 2×2 matrix form that permits analytic solutions to be obtained, and only introduces one further parameter. The approximation is that the $\vec{k}\cdot\vec{p}$ interaction of the X_1 and X_3 conduction bands with all other bands can be represented by constant mass parameters different for the two bands. The $\vec{k}\cdot\vec{p}$ interaction between X_1 and X_3 bands is then solved exactly within the usual approximation of a constant matrix element. The $\vec{k}\cdot\vec{p}$ Hamiltonian along the [001] direction is then

$$\begin{bmatrix} \frac{1}{2}\Delta+\hbar^2k^2/2m_3 & kP \\ kP & -\frac{1}{2}\Delta+\hbar^2k^2/2m_1 \end{bmatrix}, \tag{A1}$$

where Δ is the X_1-X_3 conduction-band splitting, P is the momentum matrix element multiplied by $\hbar/m_0$, and m_1 and m_3 the longitudinal masses of the X_1 and X_3 bands due to all other interactions:

$$\frac{m_0}{m_1}=1+\sum_i \frac{|\langle X_3^i|p|X_1^c\rangle|^2}{E(X_1^c)-E(X_3^i)};$$

$$\frac{m_0}{m_3}=1+\sum_i \frac{|\langle X_1^i|p|X_3^c\rangle|^2}{E(X_3^c)-E(X_1^i)}.$$

Substituting

$$1/m=\tfrac{1}{2}(1/m_3+1/m_1),\quad 1/\mu=\tfrac{1}{2}(1/m_3-1/m_1), \tag{A2}$$

the dispersion relations are found to be

$$E=\hbar^2k^2/2m\pm[(\tfrac{1}{2}\Delta+\hbar^2k^2/2\mu)^2+P^2k^2]^{1/2}, \tag{A3}$$

which reduces to the equation given by Lawaetz as $\mu\to\infty$. This gives a camel's back height of

$$\Delta E=\frac{\Delta}{2}\left(\frac{\mu}{m}-1\right)+\frac{P^2\mu^2}{\hbar^2m}-\frac{P^2m}{\hbar^2}\left(\frac{\mu^2}{m^2}-1\right)\left[\left(1+\frac{\Delta^2\hbar^2}{\mu P^2}\right)\left(\frac{\mu^2}{\mu^2-m^2}\right)\right]^{1/2}. \tag{A4}$$

Since there is an experimental value for k_0,[12] it is convenient to substitute for P in terms of k_0, which gives

$$\Delta E=-\tfrac{1}{2}\Delta+[(\tfrac{1}{2}\Delta)^2+\tfrac{1}{4}\hbar^4k_0^4(1/m^2-1/\mu^2)]^{1/2} \tag{A5}$$

and it is clear that the introduction of μ can only yield a reduced camel's back height, while we require a larger value than is found from the k_0 of Ref. 12.

In the curve fitting, we have set $\mu=\infty$ (i.e., the approximation of Ref. 13). The absorption coefficient due to an exciton with this dispersion curve is proportional to its density of states. Assuming parabolic dispersion with a constant mass m_t perpendicular to the valley axis,

$$\begin{aligned} &\alpha \propto m_t(k_+ - k_-), \quad \text{for } -\Delta E < E < 0, \\ &\alpha \propto m_t k_+, \quad \text{for } E > 0, \end{aligned} \tag{A6}$$

where

$$k_\pm^2 = (2m/\hbar^2)\{E + \tfrac{1}{2}(\Delta_0 - \Delta) \pm [\tfrac{1}{2}(\Delta_0 - \Delta)^2 + \Delta_0 E]^{1/2}\}.$$

The zero of energy is at the peak of the camel's back, and $k_\pm$ are the wave vectors corresponding to the energy E on the dispersion curve. $\Delta_0 = 2mP^2/\hbar^2$ is the value of the X_1-X_3 splitting for which the camel's back vanishes. It is clear from this expression that the line shape is only dependent on two parameters, and the effective-mass parameters only affect the intensity, which must be adjusted as the matrix element is unknown.

---

*Present address: Royal Signals and Radar Establishment, Malvern, Worcestershire WR14 3PS, United Kingdom.

†On leave from Universität Regensburg, D-8400 Regensburg, Federal Republic of Germany.

[1]N. O. Lipari and A. Baldereschi, Phys. Rev. B 3, 2497 (1971).

[2]N. O. Lipari and M. Altarelli, Phys. Rev. B 15, 4883 (1977); 15, 4898 (1977).

[3]M. Altarelli, R. A. Sabatini, and N. O. Lipari, Solid State Commun. 25, 1101 (1978).

[4]M. Altarelli and N. O. Lipari, Phys. Rev. Lett. 36, 619 (1976).

[5]A. Frova, G. A. Thomas, R. E. Miller, and E. O. Kane, Phys. Rev. Lett. 34, 1572 (1975).

[6]R. B. Hammond, D. L. Smith, and T. C. McGill, Phys. Rev. Lett. 35, 1535 (1975).

[7]M. L. W. Thewalt and R. R. Parsons, Solid State Commun. 20, 97 (1976).

[8]M. Capizzi, J. C. Merle, P. Fiorini, and A. Frova, Solid State Commun. 24, 451 (1977); and (unpublished).

[9]See, for example, Proceedings of the Thirteenth International Conference on the Physics of Semiconductors, Rome, Italy, 1976, edited by F. G. Fumi (unpublished), pp. 879–950.

[10]J. Shah, R. F. Leheny, W. R. Harding, and D. R. Wight, Phys. Rev. Lett. 38, 1164 (1977); H. Maaref, J. Barrau, M. Brousseau, J. Collet, and J. Mazzaschi, Solid State Commun. 22, 593 (1977); D. Hulin, M. Combescot, N. Bontemps, and A. Mysyrowicz, Phys. Lett. A 61, 349 (1977); D. Bimberg and M. S. Skolnick (unpublished).

[11]P. J. Dean and D. G. Thomas, Phys. Rev. 150, 690 (1966).

[12]P. J. Dean and D. C. Herbert, J. Lumin. 14, 55 (1976).

[13]P. Lawaetz, Solid State Commun. 16, 65 (1975).

[14]A. A. Kopylov and A. N. Pikhtin, Fiz. Tech. Poluprov. 11, 867 (1977) [Sov. Phys. Semiconductors 11, 510 (1977)].

[15]I. Balslev, Phys. Rev. 143, 636 (1966).

[16]L. D. Laude, F. H. Pollak, and M. Cardona, Phys. Rev. B 3, 2623 (1971).

[17]L. D. Laude, M. Cardona, and F. H. Pollak, Phys. Rev. B 1, 1436 (1970).

[18]I. Balslev, J. Phys. Soc. Jpn. 21, Suppl. 101 (1966).

[19]M. Capizzi, F. Evangelisti, P. Fiorini, and F. Patella, Solid State Commun. 24, 801 (1977).

[20]G. E. Pikus and G. L. Bir, Fiz. Tverd. Tela 1, 1642 (1959) [Sov. Phys. Solid State 1, 1502 (1959)]; G. L. Bir and G. E. Pikus, Fiz. Tverd. Tela 3, 3050 (1961) [Sov. Phys. Solid State 3, 2221 (1962)].

[21]F. H. Pollak and M. Cardona, Phys. Rev. 172, 816 1968.

[22]We choose a coordinate system with origin on a P atom. In this case the lowest conduction-band state at X, which in a tight-binding picture is composed of gallium p and phosporus s contributions, has X_1 symmetry.

[23]A. Baldereschi and N. O. Lipari, Phys. Rev. B 3, 439 (1971).

[24]E. O. Kane, Phys. Rev. B 11, 3850 (1975). (1968).

[25]E. Erlbach, Phys. Rev. 150, 767 (1966).

[26]D. L. Smith and T. C. McGill, Phys. Rev. B 14, 2448 (1976).

[27]The S-doped material was obtained from R. T. C. (Caen) and the Te-doped sample from Siemens. The Ga-Solution grown sample was kindly provided by E. Winckler and Dr. E. G. Schönherr.

[28]R. J. Elliott, Phys. Rev. 108, 1384 (1957).

[29]R. Zallen and W. Paul, Phys. Rev. 134, A1628 (1964).

[30]J. L. Yarnell, J. L. Warren, R. G. Wenzel, and P. J. Dean, *Neutron Inelastic Scattering* (IAEA, Vienna, 1968), p. 301.

[31]We have used the compliance coefficients of W. F. Boyle and R. I. Sladek, Phys. Rev. B 11, 2933 (1975) to calculate deformation potentials.

[32]J. Leotin, J. C. Ousset, R. Barbaste, S. Askenazy, M. S. Skolnick, R. A. Stradling, and G. Poiblaud, Solid State Commun. 16, 363 (1975); K. Suzuki and N. Miura, *ibid.* 18, 233 (1976).

[33]R. A. Street and W. Senske, Phys. Rev. Lett. 37, 1292 (1976).

[34]A. Onton, Phys. Rev. B 4, 4449 (1971).

[35]P. J. Dean, Phys. Rev. 157, 655 (1967).

[36]C. D. Mobsby, E. C. Lightowlers, and G. Davies, J. Lumin. 4, 29 (1971).